



NRC Publications Archive Archives des publications du CNRC

Development of a compliant and cytocompatible micro-fibrous polyethylene terephthalate vascular scaffold

Moreno, M. J.; Aji, A.; Mohebbi-Kalhari, D.; Rukhlova, M.; Hadjizadeh, A.; Bureau, M. N.

This publication could be one of several versions: author's original, accepted manuscript or the publisher's version. / La version de cette publication peut être l'une des suivantes : la version prépublication de l'auteur, la version acceptée du manuscrit ou la version de l'éditeur.

For the publisher's version, please access the DOI link below. / Pour consulter la version de l'éditeur, utilisez le lien DOI ci-dessous.

Publisher's version / Version de l'éditeur:

<https://doi.org/10.1002/jbm.b.31774>

Journal of Biomedical Materials Research Part B: Applied Biomaterials, 97B, 2, pp. 201-214, 2011-03-09

NRC Publications Record / Notice d'Archives des publications de CNRC:

<https://nrc-publications.canada.ca/eng/view/object/?id=76f83ca8-0c10-423c-82e3-f4bf88341a11>

<https://publications-cnrc.canada.ca/fra/voir/objet/?id=76f83ca8-0c10-423c-82e3-f4bf88341a11>

Access and use of this website and the material on it are subject to the Terms and Conditions set forth at

<https://nrc-publications.canada.ca/eng/copyright>

READ THESE TERMS AND CONDITIONS CAREFULLY BEFORE USING THIS WEBSITE.

L'accès à ce site Web et l'utilisation de son contenu sont assujettis aux conditions présentées dans le site

<https://publications-cnrc.canada.ca/fra/droits>

LISEZ CES CONDITIONS ATTENTIVEMENT AVANT D'UTILISER CE SITE WEB.

Questions? Contact the NRC Publications Archive team at

PublicationsArchive-ArchivesPublications@nrc-cnrc.gc.ca. If you wish to email the authors directly, please see the first page of the publication for their contact information.

Vous avez des questions? Nous pouvons vous aider. Pour communiquer directement avec un auteur, consultez la première page de la revue dans laquelle son article a été publié afin de trouver ses coordonnées. Si vous n'arrivez pas à les repérer, communiquez avec nous à PublicationsArchive-ArchivesPublications@nrc-cnrc.gc.ca.



Development of a compliant and cytocompatible micro-fibrous polyethylene terephthalate vascular scaffold

M. J. Moreno,¹ A. Ajji,^{2,3} D. Mohebbi-Kalhari,^{1,3} M. Rukhlova,¹ A. Hadjizadeh,^{2,3} M. N. Bureau^{2,4}

¹Institute for Biological Sciences, National Research Council of Canada, M54, Ottawa, ON, K1A 0R6, Canada

²Industrial Materials Institute, National Research Council of Canada, 75 Boul. de Mortagne, Boucherville, QC, J4B 6Y4, Canada

³Chemical Engineering Department, École Polytechnique de Montréal, C.P. 6079, Succursale Centre-Ville, Montréal, QC, H3C 3A7, Canada

⁴Biomedical Science and Technology Research Group (GRSTB/FRSQ), École Polytechnique, C.P. 6079, Succursale Centre-Ville, Montréal, QC, H3C 3A7, Canada

Received 26 September 2009; revised 19 August 2010; accepted 25 September 2010

Published online 9 March 2011 in Wiley Online Library (wileyonlinelibrary.com). DOI: 10.1002/jbm.b.31774

Abstract: Bioengineering approaches have been intensively applied to create small diameter vascular grafts using artificial materials. However, a fully successful, high performing and anti-thrombogenic structure has not been achieved yet. In this study, we have designed and fabricated a novel non-woven fibrous vascular graft with biomechanical properties closely resembling those of native vessels. Vascular cell growth, preservation of cell phenotype, retention of vasoactive properties, as well as the effect of gelatin coating on the cellular interaction with the scaffolds under static and shear stress conditions were investigated. The non-woven fibrous scaffolds were made from melt blown polyethylene terephthalate fiber webs stacked by means of a consolidation technique. The scaffold variables were fiber diameter distribution and the number of consolidated web stacks. SEM analysis confirmed various fiber diameter and pore size ranges corresponding to the different conditions. The scaffolds showed burst pressure values of ~ 1500 mmHg and compliance ($8.4 \pm 1.0 \times 10^{-2}\%$ mmHg⁻¹) very similar to those of native arteries ($\sim 8 \times 10^{-2}\%$

mmHg⁻¹). The structure with the smallest fiber diameter range (1–5 μm) and pore size range (1–20 μm) was the most suitable for the growth of human brain endothelial cells and aortic smooth muscle cells. The cells maintained their specific cell phenotype, expressed collagen and elastin and produced cAMP in response to α -calcitonin gene-related peptide. However, under shear stress conditions (0.9 dyne cm⁻²), only 30% of the cells were retained in both uncoated and gelatin-coated scaffolds indicating the need for improving the cell retention capacity of these structures, which is our future research direction. This study indicates that the biomechanical and biocompatible properties of this novel vascular scaffold are promising for the development of a vascular graft with similar characteristics to those of native vessels. © 2011 Wiley Periodicals, Inc. *J Biomed Mater Res Part B: Appl Biomater* 97B: 201–214, 2011.

Key Words: nonwoven PET scaffolds, melt-blowing, vascular cells, compliance, shear stress

INTRODUCTION

Vascular diseases are one of the major causes of disability and mortality in the world.¹ The standard treatment for severe vascular diseases is bypass grafting with autologous veins or arteries.² However, appropriate autologous vessels are not always available. In addition, the compliance mismatch between veins and arteries has been shown to induce long-term myointimal hyperplasia, particularly at anastomotic sites.³ To overcome these limitations, artificial vascular substitutes have been investigated as an alternative to autologous vessels.

Vascular grafts made from nonabsorbable materials such as expanded polytetrafluoroethylene (ePTFE) membranes and polyethylene terephthalate (PET) woven fibers (DacronTM) have been successfully used for replacement of large and medium diameter arteries (≥ 6 mm inner diameter).⁴ However, none of these materials have yet proved efficacy for substitution of smaller diameter conduits as they have shown to be

thrombogenic and present low patency when implanted in an arterial environment.^{5,6} They also exhibit considerably lower mechanical compliance than native arteries, which leads to a disturbed flow pattern that stimulates neointimal hyperplasia at anastomosis site.⁷ Current artificial commercial vascular grafts made of either PET fibers (woven or knitted) or ePTFE present compliance values of 1.8×10^{-2} and $1.2 \times 10^{-2}\%$ mmHg⁻¹, respectively, while compliance values in arteries, are in the order of $8 \times 10^{-2}\%$ mmHg⁻¹.^{8,9}

In search for a better artificial vascular substitutes, tissue engineering approaches have been applied to recreate the two main cellular layers of a normal artery and mimic the native vessel behavior: the intima, consisting of a monolayer of endothelial cells (ECs) that confers a thrombo-resistant surface, and the media, consisting of circumferentially aligned smooth muscle cells (SMCs) that provide most of the vascular mechanical contractibility.⁹

Correspondence to: A. Ajji; e-mail: Abdellah.Ajji@cnrc-nrc.gc.ca

Contract grant sponsor: Natural Science and Engineering Research Council Canada (NSERC)

TABLE I. Comparative Analysis of Fibre Diameter Range, Number of Web Stacks and Pore Size Range Among Five Different Nonwoven PET Structures (A–E)

Structure	A	B	C	D	E
No. of Web Stacks	10	15	20	20	20
Fibre diameter range (μm)	80% between 1–4 20% between 4–6	80% between 1–4 20% between 4–6	80% between 1–4 20% between 4–6	40% between 3–5 60% between 8–10	80% between 2–6 20% between 6–11
Average fibre diameter (μm)	3.7 ± 2.2	3.8 ± 1.2	3.6 ± 2.2	7.0 ± 2.4	5.1 ± 2.6
Pore diameter range (μm)	8–30	3–27	1–20	up to 50	1–20
Average pore diameter (μm)	16.8 ± 7.3	11.9 ± 7.2	9.0 ± 5.8	26.9 ± 13.9	10.9 ± 5.6
Average pore area (μm^2)	263 \pm 196	152 \pm 154	89 \pm 90	671 \pm 626	117 \pm 136
Solid fraction	0.14	0.19	0.27	0.31	0.30
Porosity (%)	86	81	73	69	70

To this goal, various polymers, polymer processing techniques, cell seeding methods, bioreactor culture systems,¹⁰ and designs have been employed, the most recent including pure biological constructs made of decellularized tissue,¹¹ cell sheets,¹¹ and gel constructs¹²; simple one-layer polymeric structures^{13,14} fabricated with various polymers, particularly elastomers such as polyurethane^{13,15} or polycaprolactone (PCL)^{14,16}; or hybrid multi-layer constructs¹⁷ composed of bioresorbable polymers (e.g., PCL and PGA)¹⁸ alone or in combination with ECM proteins such as collagen or elastin¹⁹ and vascular cells (i.e., ECs, SMC, and fibroblasts).¹⁸ These bioresorbable polymer-ECM protein combination approaches have been developed to profit from both the bioactivity of natural ECM proteins and the mechanical properties of synthetic polymers. However, various problems have been associated with the use of these materials^{20–22}: (i) their unsatisfactory mechanical properties (burst strength and reliability); (ii) the difficulty in matching their structural decay upon polymer degradation with vascular tissue ingrowth; (iii) the potential excessive matrix formation and stenosis related to uncontrolled tissue ingrowth; and (iv) the production of degradation products that induce dedifferentiation of SMC, stimulating chronic inflammation and inducing fibro-collagenous tissue formation that reduces graft compliance and eventually causes graft failure.

Developing a small caliber nonresorbable synthetic scaffold with optimized EC and SMC adhesive capacity to resist blood flow-related detachment²³ and retaining the normal function of the regenerated vascular tissue appears as a challenging but promising alternative to the bioresorbable vascular grafts. The long success of PET in clinical applications for large diameter vascular grafts converts it in a potential candidate to develop small-diameter vascular grafts. However, to obtain a high performing tissue-engineered small-diameter vascular graft, the compliance mismatch between the implanted graft and the vascular tissue must be resolved. This can be achieved by a suitable structural design. Among various scaffold structures, fibrous configurations allow the modulation of the mechanical properties by modifying parameters such as fiber diameter, number, and alignment of fiber webs and the consolidation method employed. Fiber structures also convey the positive contact-guidance effect of the fibers on cell migration and the capacity of modulating cell function through the typical

surface roughness created by the microfibers.^{24,25} The nature of PET allows the production of fibrous structures using fiber-spinning techniques such as melt-spinning,²⁶ electrospinning,²⁷ and melt-blowing. PET is also prone to various surface functionalization techniques such as plasma polymer deposition²⁴ and wet chemistry²⁷ by which biomolecules can be covalently grafted²⁴ to stimulate a strong cell attachment and prevent cell loss under shear stress.²⁸ Polymeric surfaces can be coated or modified with different extracellular matrix proteins such as collagen, gelatin, or fibronectin²⁹ to enhance cell attachment. For instance, methacrylic acid modified electrospun PET nanofiber mats coated with gelatin showed improvement of the spreading and proliferation of the ECs and preservation of their phenotype.²⁷

The aim of this study was to create novel vascular matching compliant structures to be used as small diameter scaffolds using PET, a widely used and clinically accepted polymer. To this end, we used melt-blowing, a high throughput, cost-effective fabrication method which allows high control over fiber diameter distribution and pore size range. EC and SMC viability, growth, phenotype, cell retention under shear-stress conditions and vasoactive function were assessed in uncoated and gelatin-coated scaffolds along with the strength and mechanical behavior of these nonwoven PET fiber structures.

MATERIALS AND METHODS

Preparation of nonwoven PET fiber structures

Neat PET (Dupont, Wilmington, DE, USA), with an inherent viscosity of 1, was used to produce nonwoven fibers using the melt-blowing process. PET was extruded through a die containing 230 aligned holes (ca. 300 μm in diameter). Air was blown at very high speed (close to the speed of sound) through a narrow gap sideways of the die and allowed for stretching of the fibers. The fiber diameter was changed by varying the flow rate of the molten polymer (ranges used varied from 0.5 to 6 kg h^{-1}). The fibers were then used to prepare five desired nonwoven PET fiber structures, designated as A–E (Table I) for the study. Planar scaffolds were prepared for EC and SMC culture and tubular scaffolds for mechanical testing. They were elaborated by juxtaposition of various numbers of individual layers of fiber webs with alternating orientations ($0^\circ/90^\circ$) onto a metallic plate or a 6-mm diameter mandrel. The plate was placed into an

autoclave and the mandrel sealed in a vacuumed bag and then inserted in an oven with controlled temperature (100°C) and under vacuum conditions (100 kPa) during 20 min for consolidation.

Morphological analysis of nonwoven PET fiber structures

A field emission scanning electron microscope (FE-SEM, S-4700, Hitachi High-Technologies Canada, Toronto, Canada) was used for observation of the fibers and structures. FE-SEM images from the planar surface of the scaffolds as well as from the cross sections were taken. The fiber diameter and pore size range were determined from at least five SEM at a magnification of $500\times$ ($N > 200$ fibers) using an image analysis software (Visilog 5, Noesis, Les Ulis, France). The porosity, p , of the scaffolds was calculated from the following equation:

$$p = 1 - \frac{\rho_s}{\rho_0} = 1 - \frac{(M_s/V_s)}{\rho_0} \quad (1)$$

where ρ_s and ρ_0 are respectively the density of the scaffold and the base polymer, and M_s and V_s are the mass and the volume of scaffold disks (nominal 10-mm diameter) used to calculate ρ_s . ρ_0 was obtained from PET supplier. Measurements were done in triplicates for each scaffold.

Mechanical testing

Compliance measurements on tubular scaffolds were performed on a custom-made compliance testing device. This tester consists in a rod-mounted inflatable balloon connected to a pressurized nitrogen line via a pressure regulator. The tubular scaffolds were inserted onto the rod-mounted balloon. Data acquisition of both applied pressure and the scaffold diameter variation upon pressure application was performed. The pressure was monitored through a pressure transducer (AP-34K, Keyence Canada, Mississauga, Canada). The scaffold diameter was measured using a laser scanner (LS-3100, Keyence Canada).

The scaffold specimens tested were 5 cm in length and 6.35 mm in outer diameter. They were submitted to pressure cycles between 0 and 200 mmHg, at an approximate rate of 100 mmHg s^{-1} . Scaffolds were submitted to 100 consecutive pressure cycles for preliminary mechanical integrity assessment. Pressure-diameter measurements were collected at a rate of 10 points per second. Measurements of compliance, C , were made from the pressure-diameter curves according to Eq. (2)³⁰:

$$C = (\Delta D/D_0 \cdot \Delta P) \times 10^4 \quad (2)$$

where ΔD refers to the variation of diameter when a variation of pressure ΔP is applied to a scaffold with an initial diameter D_0 . The compliance of the tubular scaffolds studied was compared with those measured on two commercial vascular grafts, ePTFE and Dacron. Finally, burst pressure measurements were performed on the tested tubular scaffolds (nonwoven PET fiber structures) and commercial

vascular grafts by increasing the internal pressure at a rate of 100 mmHg s^{-1} .

For mechanical testing, comparative analysis was made with ePTFE (IMPRA Carboflo[®], 6 mm, Bard Peripheral Vascular, Tempe, AZ) and Dacron (Hemashield Platinum, Woven Double Velour, 6 mm, Boston Scientific, Wayne, NJ) tubular structures. For cell culture, these materials were not investigated due to the following reasons: (i) the hydrophobic nature of unmodified ePTFE material does not allow cell seeding on these structures, (ii) the corrugated surface of commercial Dacron does not allow a comparative analysis with non-corrugated PET structures.

Cell cultures

Human brain endothelial cells (HBECs) were obtained from small intracortical microvessels and capillary fractions (20–112 μm) harvested from human temporal cortex excised surgically from patients treated for idiopathic epilepsy as described previously.³¹ Tissues were obtained with approval from the Institutional Research Ethics Committee. HBECs were seeded on 0.5% gelatin-coated polystyrene Falcon culture plates (PFPC), separated from contaminating smooth muscle cells (SMCs) with cloning rings, cultured and routinely characterized morphologically and biochemically as previously described.³¹

Human aorta smooth muscle cells (AoSMC) were obtained from Clonetics (Walkersville, MD). Cells were seeded on PFPC and cultured in smooth muscle growth media (SmGM[®]-2 BulletKit[®], Clonetics, Walkersville, MD) in a standard incubator until reached about 80% confluence. More than 95% of the AoSMC in cultures stained immunopositive for the smooth muscle marker α -actin.

HBEC and AoSMC cellular adhesion and growth evaluation

HBEC and AoSMC were respectively trypsinized with 1 mL of either GRP-2 (Cells systems, Kirkland, WA) or GIBCO (0.25%) trypsin. Planar discoidal scaffolds (11-mm diameter) were sterilized by incubation in 200 U mL^{-1} penicillin and 200 $\mu\text{g mL}^{-1}$ streptomycin overnight, then washed thoroughly in HBSS, placed in Falcon 24-well plates and pre-wetted overnight with either 0.5% gelatin (for HBEC) or cell media (for AoSMC). About 50 μL of culture media containing either 5×10^5 HBEC or 10^6 AoSMC were applied to the scaffolds and let them sit for 20 min before filling the wells with additional 450 μL of media. Cells were allowed to grow on the scaffolds for 6 days in a standard incubator. To visualize and quantify the number of living cells on the planar discoidal scaffolds, cells were washed with warm HBSS, incubated with 10 $\mu\text{g mL}^{-1}$ carboxy-fluorescein diacetate acetoxyethyl ester (CFDA-AM) (Molecular Probes, Frederick, MD) at 37°C for 45 min and washed again with HBSS. Fluorescence of the cell-seeded scaffolds was measured at 485/530 nm using a cytofluorimeter plate reader (Bio-Tek FL600, Winooski, VT) and the autofluorescence emitted by the scaffolds alone subtracted. Two separate experiments with triplicate samples ($n = 6$) were performed on the uncoated and gelatin-coated structures tested.

TABLE II. Summary of Hemodynamic Parameters Used to Evaluate Cell Retention Under Shear Stress

Input Parameters	Value	Computed Parameters	Value
Frequency of pulsatile cycle (Hz)	1	Womersley number	5.8
Internal diameter (mm)	4.7	Mean shear stress (steady flow)(dyne cm ⁻²)	0.90
Mean flow rate (mL min ⁻¹)	50	Mean shear stress (pulsatile flow)(dyne cm ⁻²)	0.93
Mean pressure (mmHg)	100	Entrance length (mm)	58.7
Pressure (mmHg)	120/80	Reynolds number	228.5
Viscosity (poise)	0.01		
Temperature (°C)	37 ± 1		
pH	7.3 ± 1		

Proliferation assay

Proliferation of HBEC and AoSMC were determined using CyQUANT[®] cell proliferation assay kit (Molecular Probes). Briefly, 4×10^4 cells/well (HBEC) and 2×10^3 cells/well (AoSMC) were seeded on either uncoated or gelatin-coated scaffolds or in PFCP. Cells were harvested at either 8, 24, 48, and 96 h (for HBEC) or 8, 24, 48, and 72 h (for AoSMC) by washing with HBSS, blotting microplates dry, and storing at -80°C until analysis. Plates were thawed at room temperature; 300 μL of CyQUANT GR dye/lysis buffer were added to each well for 5 min in the dark. Fluorescence values measured in a cytofluorimeter plate reader at 485/530 nm were converted into cell numbers from cell reference standard curves. Two separate experiments with triplicate samples ($n = 6$) were performed on uncoated and gelatin-coated structure E.

HBEC retention under steady and pulsatile shear stress conditions

The effect of shear stress on the retention of HBEC (10^5 cells/scaffold) by uncoated and gelatin-coated PET planar scaffolds short after (4 h) cell seeding was evaluated. The scaffolds were placed under sterile conditions into the luminal side of a silicone tube. The tube was then fixed to the grips of a culture chamber of a LumeGen Bioreactor (Tissue Growth Technologies; Minnetonka, USA). A schematic of the bioreactor system is shown in Figure 8. Culture media was circulated through the lumen of the tube for 10 min using a peristaltic pump (Cole-Parmer, Montreal, Canada) at a laminar flow rate of 50 mL min⁻¹ and a mean pressure of 100 mmHg. A set of scaffolds was submitted to physiological pressure (120/80 mmHg) using a pulsatile pressure stimulator (Tissue Growth Technologies). In the control group, cells seeded on the uncoated and gelatin-coated scaffold were maintained in the culture plates under static conditions.

Shear stress values on the scaffolds under steady and pulsatile pressures were respectively estimated using the Poiseuille (3) and Womersley (4) formulas,^{32,33} and the input parameters summarized in Table II.

$$\tau_{w,s} = \frac{4\mu Q}{\pi R^3} \quad (3)$$

$$\tau_{w,p} = \frac{\alpha}{\sqrt{2}} \left(\mu \frac{U}{R} \right) \quad (4)$$

where μ is the culture media viscosity, R is the tube radius, Q is the volumetric flow, U is the volumetric velocity, and α

is the nondimensional Womersley number. The Womersley number was calculated from Eq. (5), where ω is angular velocity of pulsation, ν is kinematics viscosity, and R is tube radius.

$$\alpha = R \sqrt{\frac{\omega}{\nu}} \quad (5)$$

The calculation of the entrance length was obtained from the following Eq. (6),³⁴ where L_e is the entrance length and ρ is the fluid density.

$$L_e = 0.226 \frac{\rho UR^2}{\mu} \quad (6)$$

Based on these parameters, cells under steady and pulsatile pressure conditions were submitted to shear stress values of 0.90 and 0.926 dyne cm⁻², respectively. This range of physiological shear stress has been shown to enhance endothelial cell function.^{35,36}

After exposure of the cells to 10 min of shear stress, the scaffolds were removed from the lumens of the silicone tubes and placed in a 12-well plate for cell quantification using Alamar Blue[®] assay, a method previously used for monitoring cell viability and retention *in vitro*.^{37,38} Alamar Blue (AbD Serotec, Oxford, UK) was added to the cells at a 5% final concentration and incubated at 37°C in dark for 4 h. Media (500 μL) was transferred to a new plate, fluorescence intensity was monitored at 530/590 nm wavelengths using a fluorescence plate reader. Fluorescence values were converted into cell numbers from cell reference standard curves.

HBEC and AoSMC cellular phenotype analysis

To determine whether the interaction of vascular cells with the scaffolds may affect their phenotype, the presence of specific endothelial (Factor VIII expression and Ulex Europaeus I lectin binding) and smooth muscle cell (α -actin expression) markers was analyzed in cells seeded for 5 days on the nonwoven PET scaffolds. Expression of collagen and elastin, two main matrix components of the vascular wall, were also investigated. HBEC and AoSMC grown on nonwoven fiber scaffolds were fixed with 4% paraformaldehyde for 10 min at room temperature. Cells were then rinsed with HBSS, and permeabilized with 0.1% Triton X-100 (EM Science Gibbstown, NJ) in HBSS at room temperature for 10 min. After rinsing, cells were blocked with 4% serum

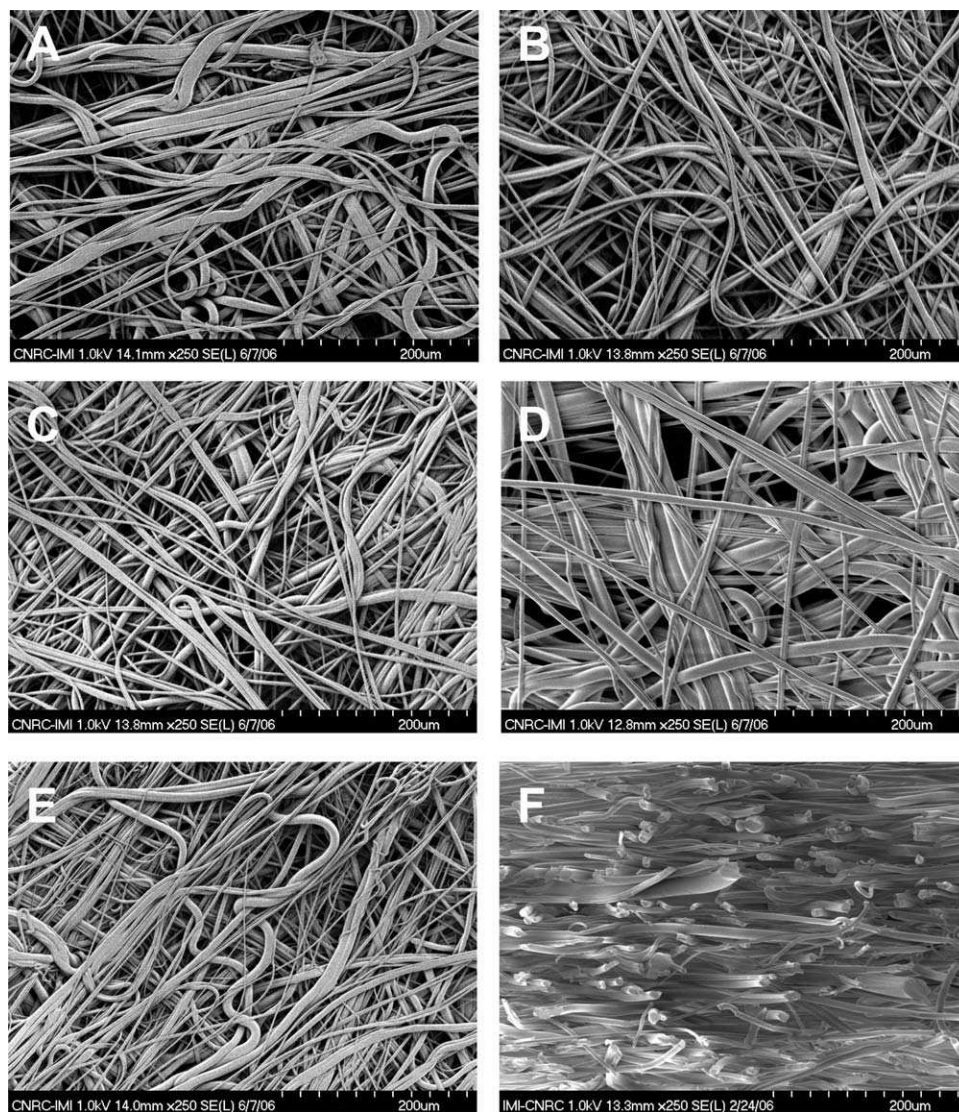


FIGURE 1. SEM images of the different nonwoven PET fiber scaffolds (A, B, C, D, and E) investigated. F is a representative cross-section of the scaffolds.

in HBSS for 1 h at room temperature. HBEC were then incubated with either primary rabbit anti-human von Willebrand Factor (1:500 dilution, DAKO, Denmark, Copenhagen) or mouse anti-human collagen IV (1:500 dilution, Abcam, Cambridge, MA) antibodies for 1 h at room temperature. Cells were rinsed with HBSS and respectively exposed to secondary goat anti-rabbit Alexa Fluor 488 (1:500 dilution, Molecular Probes, Burlington, ON, Canada) or goat-anti-mouse Alexa Fluor 568 (1:500 dilution, Molecular Probes) antibodies for 30 min at room temperature. Samples stained with anti-human collagen IV were also exposed to Fluorescein Ulex Europaeus Agglutinin-1 (1:50 dilution, Vector Lab., Burlingame, CA) for 30 min. AoSMC were incubated with primary mouse anti-human α -smooth muscle actin (1:500 dilution, R&D systems, Minneapolis, MN) and rabbit anti-human elastin (1:500, Ciderlan, Hornby, ON, Canada) for 1 h at room temperature. Cells were respectively exposed to goat anti-mouse Alexa Fluor 568 (1:500 dilution) or goat

anti-rabbit Alexa Fluor 488 (1:500 dilution, Molecular Probes) for 30 min at room temperature. Cells were rinsed twice with HBSS and covered with DAKO mounting media spiked with DAPI ($2 \mu\text{g mL}^{-1}$, Sigma, Okville, ON, Canada) and placed on glass slides. Fluorescence images of the cells attached to the scaffolds were obtained using a fluorescence microscope (Olympus 1X50; Carsen group, Markham, ON, Canada) Images were captured using a digital video camera (Olympus U-CMT) and analyzed with Northern Eclipse v.5.0 software (Mississauga, ON, Canada). Two separate experiments with triplicate samples ($n = 6$) were performed on structure E.

Cyclic adenosine monophosphate (cAMP) production

To investigate whether HBEC grown for 6 days on the PET planar scaffolds retain their ability to respond to vasoactive agents, the effect of increasing concentrations (50–1000 nM) of the potent vasodilator α -calcitonin gene-related peptide (CGRP) on cAMP production in HBEC was assayed.

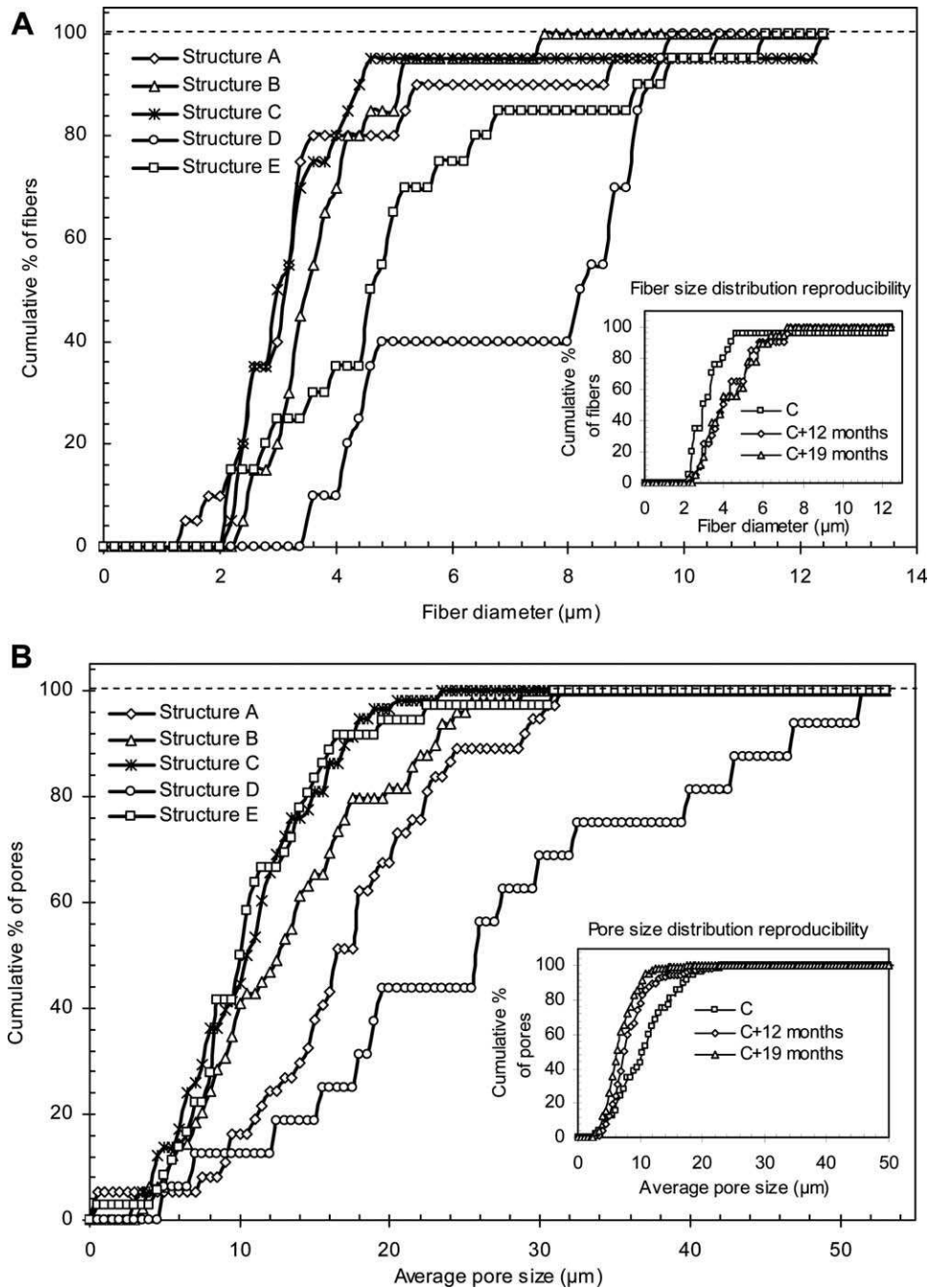


FIGURE 2. (A) shows fiber diameter distribution of the different nonwoven PET fiber scaffolds (A, B, C, D, and E), represented by the cumulative relative distribution (in % of population) of fibers as a function of fiber diameter. (B) Pore size distribution of the scaffolds (A, B, C, D, E), represented by the cumulative relative distribution (in % of population) of pores as a function of the pore diameter. The inserts in the Figure 2(A,B) show the respective reproducibility of fiber diameter and pore size distribution measurements for the same structure made at different times (structure C in example shown).

This effect was compared to that obtained on HBEC grown on gelatin-coated 24-well-PFCP as a control. At day 6, media was removed; cells were washed with HBSS and incubated in phosphate buffered saline (PBS) containing 0.2% bovine serum albumin and 1 mM 3-isobutyl-1-methyl-xanthine for 10 min before application of CGRP. Determination of cAMP content was performed using a commercial Amersham

cAMP Biotrak Enzymeimmunoassay System (GE Healthcare, Buckinghamshire, UK) as previously described.³⁹ The cell pellets were dissolved in 0.1 N NaOH, protein levels measured by Lowry method, and production of cAMP expressed as function of protein content. Two separate experiments with triplicate samples ($n = 6$) were performed on the uncoated and gelatin-coated scaffolds.

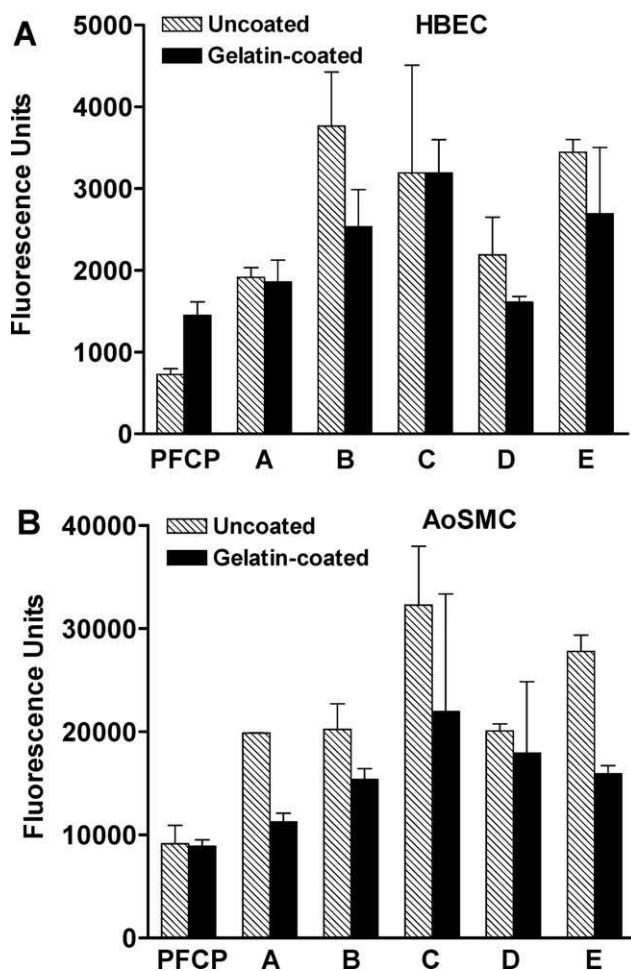


FIGURE 3. Vital staining with CFDA-AM of HBEC (A) and AoSMC (B) grown for 6 days on uncoated (hatched bar) or gelatin-coated (black bar) nonwoven PET fiber structures (A, B, C, D, E, F). Bars represent mean of fluorescent units (485 nm ex/530 nm em) \pm SD of two experiments performed in three scaffolds per structure ($n = 6$).

Statistical analysis

Results were expressed as mean \pm standard deviation. Data were analyzed by one-way analysis of variance (ANOVA) followed by Newman Keule's *post hoc* test at the confidence level of 95%.

RESULTS

Structure characterization

In this study, five different nonwoven PET structures (designated scaffolds A to E) were fabricated using a melt-blowing process. FE-SEM images obtained from both planar surfaces and cross-sections were used to determine the fiber diameter and pore size ranges of the five different structures. The structures differ in fiber diameter range and number of fiber web stacks (Table I). Micrographs of structures A to E are shown in Figure 1(A–E), and a typical cross-section micrograph is shown in Figure 1(F). Figure 2(A) shows the cumulative relative distribution of fibers as a function of fiber diameter. Structures A, B, and C show similar fiber diameter distribution with $\sim 80\%$ of the fibers in the 1- to

4- μm diameter range and $\sim 20\%$ between 4 and 6 μm . The insert-graph in Figure 2(A) illustrates the reproducibility in fiber diameter distribution measurements for two different batches of structure C. Structure D has the largest distribution of fiber diameters with $\sim 40\%$ of the fibers with diameter between 3 and 5 μm and $\sim 60\%$ between 8 and 10 μm , while structure E has $\sim 80\%$ of its fibers in the 2- to 6- μm diameter range and $\sim 20\%$ between 6 and 11 μm . Figure 2(B) shows the cumulative relative distribution of pore sizes as a function of their average equivalent diameter (calculated using the assumption that the pore shape is circular for comparison purposes). Structures A, B, and C present similar fiber diameter range but differ in the number of fiber web stacks ($A = 10$, $B = 15$, $C = 20$), which, as shown in Figure 2(B), has a direct effect on the average pore size of the structures. Structure A (10 web stacks) show a pore size range between 8 and 30 μm , structure B (15 web stacks) between 3 and 27 μm and structure C (20 web stacks) between 1 and 20 μm . Structures E and C (20 web stacks each) present similar pore size range with minor differences at the low end, whereas structure D shows a large range in pore sizes and the largest pores (up to 50 μm). Reproducibility of the pore size measurements for two different batches of structure C are illustrated in the insert-graph in Figure 2(B).

EC and SMC attachment and growth

The ability of EC and SMC to adhere and grow on the nonwoven PET scaffolds was evaluated in both uncoated and gelatin-coated scaffolds. Viability studies were performed by staining the cells with the vital dye CFDA-AM. As shown in Figure 3, while HBEC grew more efficiently ($p < 0.05$) in gelatin-coated than in uncoated PFCP, AoSMC growth was not affected by PFCP coating with gelatin. All structures allowed attachment and growth of both HBEC and AoSMC. Structures A and D, presenting the highest pore size, were the less permissive ($\sim 30\text{--}50\%$ lower fluorescence readings, $p < 0.05$) to the growth of both HBEC and AoSMC [Figure 3(A,B)]. HBEC grew with similar efficacy in structures B, C, and E [Figure 3(A)], while AoSMC growth was more efficient ($p < 0.05$) in structures C and E [Figure 3(B)]. Structure E showed more reproducibility in HBEC and AoSMC growth than structure C. Interestingly, HBEC grew with similar efficacy on uncoated and gelatin-coated structures [Figure 3(A)], while the growth of AoSMC was similar (structures C and D) or significantly lower ($\sim 20\text{--}50\%$ in structures A, B, and E, $p < 0.05$) in gelatin-coated scaffolds [Figure 3(B)].

Cell proliferation studies

Viability studies indicated that structures C and E were the most efficient for the growth of both HBEC and AoSMC, however, structure E exhibited higher reproducibility than C among the different experimental repeats. Therefore, a more detailed analysis of HBEC and AoSMC proliferation was performed in uncoated and gelatin-coated structure E. As shown in Figure 4(A), HBEC proliferation in structure E was time-dependent. Although HBEC growing on gelatin-coated scaffolds proliferate ~ 2 -fold faster in the first 24 h compared to those growing on uncoated scaffolds, the cells reached the

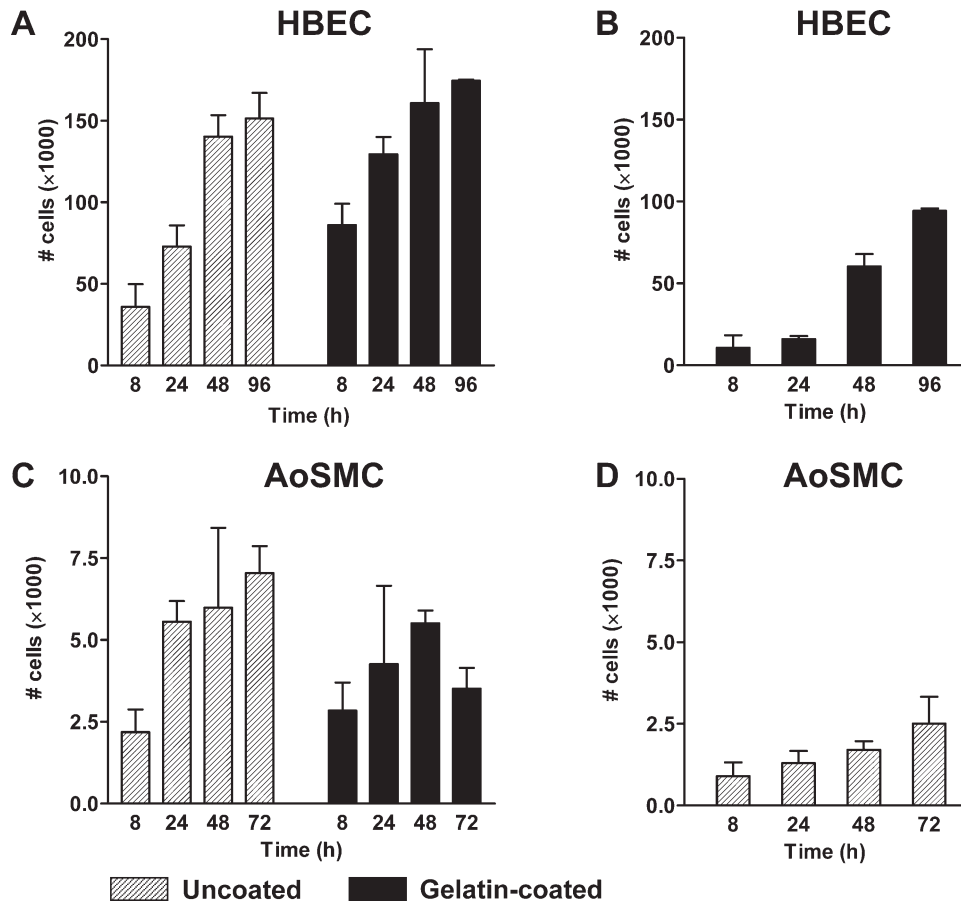


FIGURE 4. Proliferation rates of HBEC (A) and AoSMC (C) grown on either uncoated (hatched bar) or gelatin-coated (black bar) nonwoven PET fiber scaffolds of structure E or on gelatin-coated (HBEC, B) and uncoated (AoSMC, D) PFPC wells. Number of cells was quantified using CyQuant Proliferation Kit. Bars represent mean \pm SD ($n = 6$). * Indicates significance ($p < 0.05$) relative to the initial time point (8 h). # Indicates significance ($p < 0.05$) relative to the corresponding time-point between uncoated and gelatin-coated scaffolds.

same maximum number in both uncoated and gelatin-coated scaffolds after 96 h of incubation. In gelatin-coated PFPC with wells of the same diameter the number of HBEC at 96 h was 1.5-fold lower than in uncoated and gelatin-coated scaffolds. However, the initial (8 h) number of HBEC present in the wells was also significantly reduced compared to those in the scaffolds, which could indicate that the initial attachment is perhaps lower in the wells [Figure 4(A,B)]. AoSMC growth was similar in the uncoated and gelatin-coated scaffolds [Figure 4(C)], which was 3-fold higher than that in uncoated PFPC with wells of similar diameter [Figure 4(C,D)].

Effect of steady laminar and pulsatile shear stress conditions on HBEC retention

The effects of both steady laminar and pulsatile shear stress conditions on HBEC retention by uncoated and gelatin-coated scaffolds were evaluated short after seeding, using an adapted bioreactor flow circuit to generate laminar and physiological pulsatile shear stress conditions [Figure 5(A-C)].

As shown in Figure 8(D), cell retention in uncoated PET scaffold E submitted to 10 min of either steady laminar or pulsatile shear stress was respectively reduced to ~ 30 and

21% when compared to the control (static) group. The same effect was observed in gelatin-coated scaffold E, where cell retention dropped to $\sim 38\%$ (steady laminar shear stress) and 24% (pulsatile shear stress) compared to the control (static) condition. The reduction in cell retention between uncoated and gelatin-coated scaffolds was not significantly different ($p > 0.05$) under any of the shear stress conditions applied.

HBEC and AoSMC cellular phenotype

HBEC and AoSMC stained with the vital dye CFDA-AM showed attachment to the nonwoven PET fiber scaffolds. The cells were elongated and aligned following the direction of the fibers [Figure 6(A,B)]. After 6 days, the structure appeared completely populated with cells that spread through the scaffold [Figure 6(C-E)] and retained their specific molecular markers; HBEC expressed factor VIII [Figure 6(C)] and bound Ulex Europaeus I lectin [Figure 6(D,E)] and AoSMC expressed α -actin [Figure 6(F,G)]. In addition, HBEC expressed collagen IV [Figure 6(E)], an ECM protein that provides tensile integrity to the inner layer (intima) of the vascular wall, and

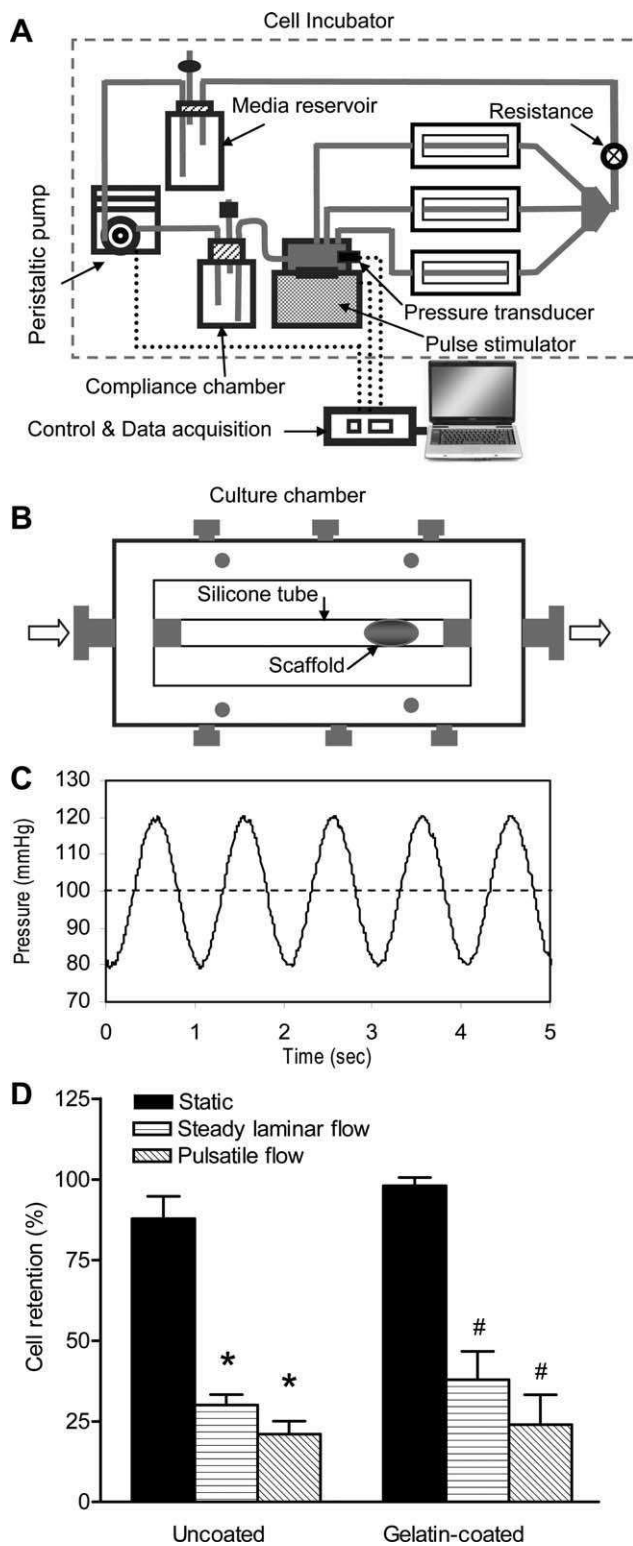


FIGURE 5. (A) A schematic of the pulsatile bioreactor system. (B) Position of the planar scaffold E in the lumen of a silicone tube fixed to the grips of a bioreactor culture chamber. (C) A representative image of the pressure waveform applied to the scaffolds. (D) Histogram representing the retention of HBEC seeded onto uncoated and gelatin-coated PET planar scaffold E after exposure to either steady or pulsatile shear stress. Bars represent mean of cells retained in the scaffolds \pm SD ($n = 3$). * $p < 0.05$ between shear stress versus static conditions in uncoated scaffolds and # $p < 0.05$ between shear stress and static conditions in coated scaffolds.

AoSMC expressed elastin [Figure 6(G)], an ECM responsible for elastic recoil of arteries.

CGRP-induced cAMP production on HBEC

The ability of HBEC grown on scaffolds of structure E for 6 days to produce cAMP upon stimulation with different concentrations of CGRP was analyzed and compared to that of HBEC grown for the same period of time on gelatin-coated PFCP (Figure 7). The basal levels of cAMP were similar between HBEC grown on uncoated scaffolds of structure E and gelatin-coated PFCP, with values ranging between 180 and 280 fmol μg^{-1} prot. In both cultures, CGRP elicited a dose-dependent production of cAMP, with a maximum effect at 100 nM (4- to 6-fold above basal levels, $p < 0.05$), as shown in Figure 7. No statistically significant differences were obtained in the cAMP production between HBEC grown on gelatin-coated PFCP and uncoated scaffolds of structure E at any concentration of CGRP tested.

Scaffold compliance

The compliance of tubular structures was measured using a custom-made set-up as described in Materials and Methods section. The tubular scaffolds were subjected to 100 pressure cycles (between 0 and 200 mmHg). Pressure-diameter curves are reported for cycle 1, 5, 10, 30, 50, and 100 (Figure 8). These pressure-diameter curves all show a steep increase at an approximately constant radial deformation, followed by a non-linear behavior with typical two-stage "J" shape pressure-diameter curves, characterized by a first stage in the 80–120 mmHg range followed by a second stage with a steeper slope in the 120–200 mmHg.⁴⁰ For all 100 cycles imposed, the scaffolds exhibit an approximately constant compliance (initial slope) within the first stage in the 80–120 mmHg range and do not exhibit cumulative deformation (creep or fatigue-like), as its radial deformation is stable and ranged between 0.08 and 0.15–0.16 mm mm^{-1} as internal pressure is applied.

The compliance values obtained for nonwoven PET fiber scaffolds are comparable to those reported for native arteries and ~ 7 and 8 times higher than those obtained for Dacron and ePTFE grafts, respectively (Table III). Burst pressures values for nonwoven PET fiber scaffolds are in the order of those reported for the human saphenous vein but slightly below the burst pressure values reported for human arteries (Table III).

DISCUSSION

PET and PTFE are two polymers that are successfully used as large diameter vascular grafts for peripheral vascular surgery; however, they are not suitable for small-diameter vascular applications as they suffer from either early occlusion or late intimal hyperplasia. Thrombogenicity and compliance mismatch of prosthetic graft at the anastomosis site have been implicated as the two major causes of the early and late graft failure, respectively. Consequently, major attempts are being conducted to both lining the lumen of vascular grafts with endothelial cells to reduce thrombogenic responses and

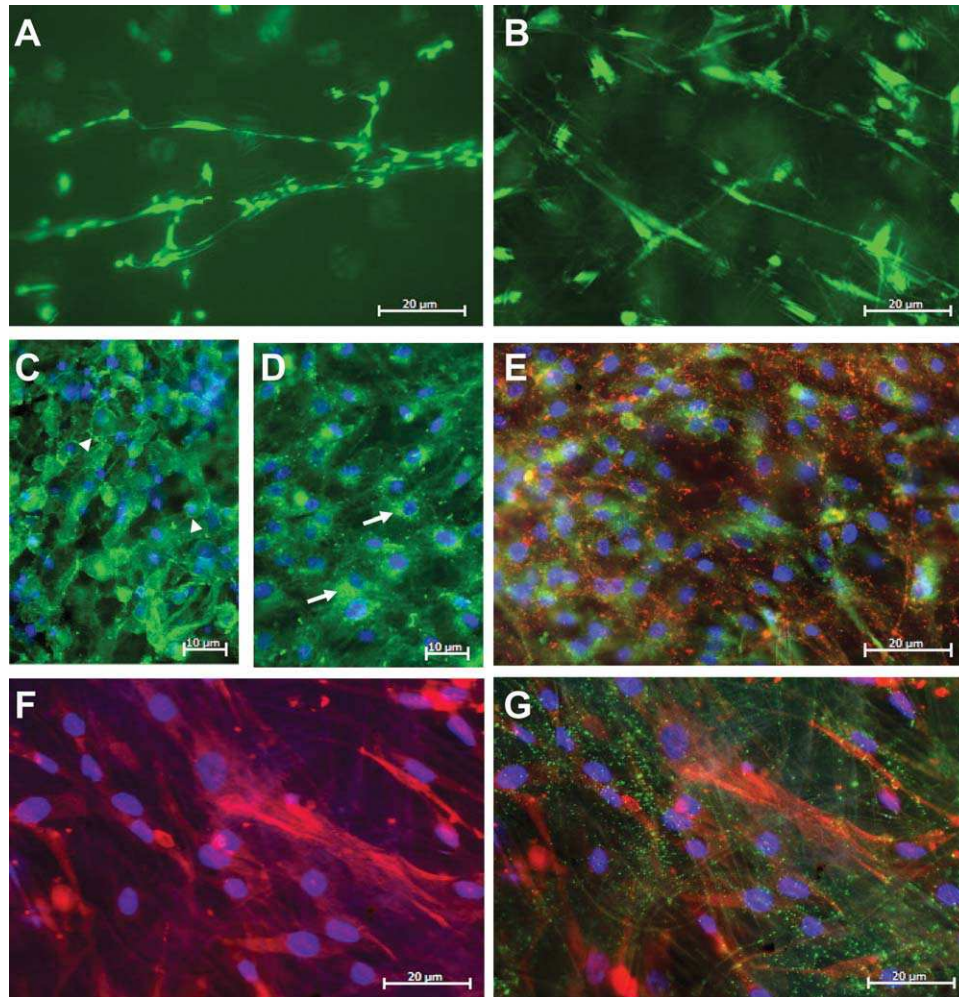


FIGURE 6. Fluorescence images of HBEC (A, C, D, and E) and AoSMC (B, E, F, and G) growing on the nonwoven PET fiber scaffolds. HBEC (A) and AoSMC (B), stained with the vital dye CFDA-AM, attached to the nonwoven PET fiber scaffolds with the cell body elongated following the direction of the fibers. HBEC labeled with fluorescein-conjugated UEA-1 (green) (C) showed marked staining surrounding the plasma membrane (head arrow). HBEC immunofluorescently-labeled with antibodies against Factor VIII related-antigen (D) showed intracellular granular staining (arrow). HBEC stained with fluorescein-conjugated UEA-1 (green) and antibodies against type IV collagen (red) (E). Immunostaining of AoSMC with antibodies against anti-smooth muscle α -actin (red) (F and G) and anti-elastin antibodies (green). Cellular nuclei were stained with DAPI (blue) (C, D, E, F, and G). Scale bars for A, B, E, F, G is 20 μm and for C and D is 10 μm .

to develop compliant-matching vascular materials to avoid intimal hyperplasia.

In this study, five different nonwoven PET fiber structures were fabricated using a melt-blowing process and their morphological, mechanical and cytocompatibility properties analyzed for their potential use in small diameter vascular applications. This fabrication method allows the control of the fibrous structure pore size and porosity as well as mechanical compliance adjustment of the scaffolds. This manufacturing process is much more cost effective than many other methods. The five nonwoven PET structures produced in this study differed in fiber diameter distribution (1–11 μm) and number of web stacks (10, 15, or 20 webs), which directly affected the pore size distribution (from 1–20 to up to 50 μm) and the total porosity (from 61.2 to 86.3%) of the scaffolds.

In tissue engineering, scaffold materials provide a mechanical support for cell growth and tissue formation.

Woven or knitted PET fibers (Dacron) and ePTFE membrane vascular grafts are poor substrates for cell attachment^{44,45}, requiring coating with cell adhesion moieties to enhance the strength and kinetics of cell attachment. However, it has been shown that scaffolds with large surface areas, porous microstructures, and interconnected pores have better cell attachment and tissue growth, compared to nonporous materials.^{46,47} Porosity is also required for intercellular exchange of cytokines and growth factors produced by both EC and SMC. The nonwoven PET fiber grafts fabricated in our laboratory are porous structures, with controllable fiber diameter distribution and narrow pore size range of 1–20 μm (structure E). This pore size range is comparably smaller than that reported for woven Dacron grafts (inter-fiber spacing of \approx 5–10 μm and inter-yarn spacing of \approx 50–100 μm)^{46,47} and of similar range (internode distance \sim 18–24 μm) than that reported for the commercial ePTFE grafts used in this

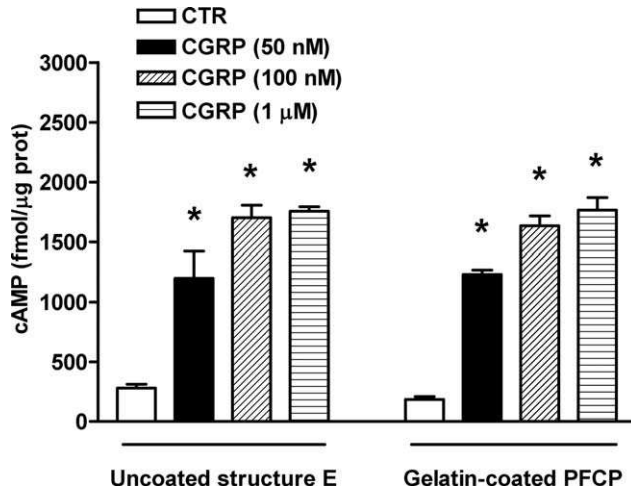


FIGURE 7. Effect of different concentrations of CGRP on cAMP production in HBEC grown on either gelatin-coated PFCP or uncoated nonwoven PET fiber scaffolds of structure E. Bars are means \pm SD ($n = 6$). *Indicates significance ($p < 0.05$) relative to the corresponding static condition.

study.^{46,47} Cell growth comparison between the five nonwoven PET fiber scaffolds showed that the structures displaying the smallest fiber diameter (1–6 μm , structures C and E), pore size distribution (1–20 μm , structures C and E) and average pore area (~ 90 and $115 \mu\text{m}^2$ for structures C and E, respectively) were the most suitable for the growth of both HBEC and AoSMC, an effect maybe due to the trapping of the cells in the small pores during the seeding step. Structure E was, however, selected for further analysis, as it exhibited higher reproducibility in HBEC and AoSMC growth than structure C. Although structure E shows promising results in terms of cell adhesion and proliferation, a more detailed anal-

ysis of SMC penetration and cellular interconnectivity will be required to ensure the correct assembly and orientation of the collagen fibers within the scaffold and to obtain the tensile strength necessary for vascular graft applications.

Several studies have demonstrated increased efficacy in EC adhesion and growth on gelatin-impregnated biomaterials⁴⁸; however, our studies showed no improvement (HBEC) and even a reduction (AoSMC) in cell growth on gelatin-coated scaffolds, which underscores the good interaction between the vascular cells and the uncoated nonwoven PET fiber scaffolds. Under steady laminar and pulsatile flow conditions, cell retention to the uncoated scaffold E was significantly reduced (60–79%) compared to the static conditions. The evaluation of cell retention was performed using shear stress values of similar magnitude than those estimated in the fetal descending aorta⁴⁹ and applied after a short period of rest (4 h) following cell seeding. The purpose of using this protocol was to evaluate cell retention during the first phase of initial contact and cell spreading on the uncoated scaffolds and compare it to that obtained in gelatin-coated ones. Retention on the nonwoven PET scaffolds was similar or superior to that previously reported in PET and ePTFE under relatively similar conditions.^{35,50} Our data indicate that there is no improvement on cell retention in gelatin-coated scaffolds compared to that obtained in uncoated ones in either of the shear stress conditions applied. Various flow and shear-stress loading protocols have been investigated^{51,52} to maximize the long-term cell retention on various scaffolds under laminar and pulsatile flow conditions. Application of more selective protocols to gradually increase shear stress after cell seeding may yield better long-term cell retention on these novel scaffolds.

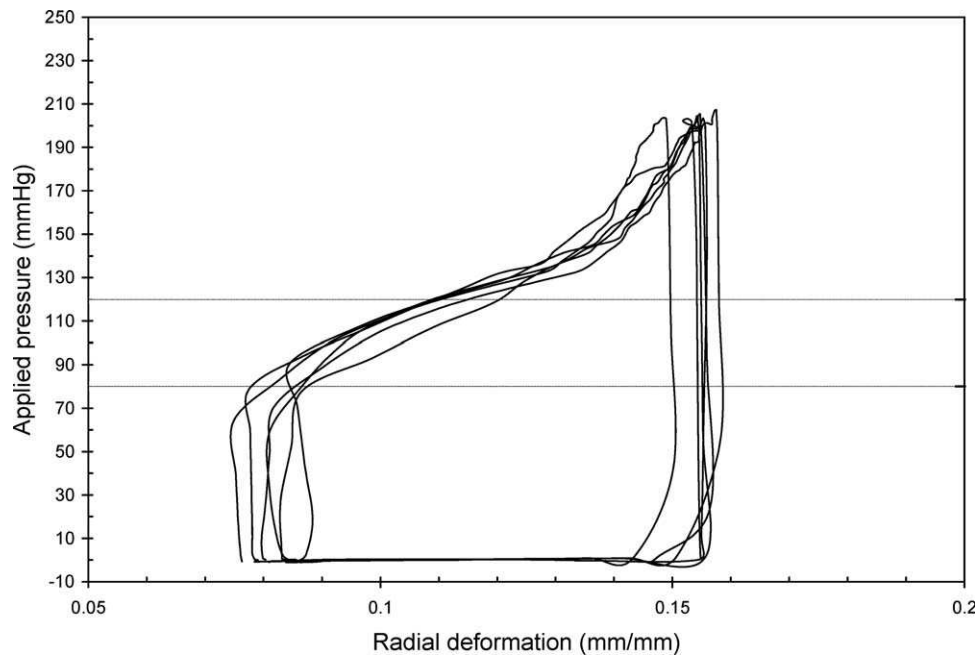


FIGURE 8. Pressure-deformation curves obtained from tubular nonwoven PET fiber scaffolds at cycle 1, 5, 10, 30, 50, and 100. Horizontal lines indicate systolic/diastolic pressure range in which compliance and modulus are measured

TABLE III. Compliance and Burst Pressure Values Measured on Nonwoven PET Structure E, Commercial Dacron, ePTFE Grafts, and Reported Human Vessels

Materials	Compliance (% mmHg ⁻¹)	Burst Pressure (mmHg)
Nonwoven PET fiber scaffold E (<i>n</i> = 3)	$8.4 \pm 1.0 \times 10^{-2}$	1509 ± 175
Dacron grafts (<i>n</i> = 2)	$1.1 \pm 0.2 \times 10^{-2}$	4145 ± 207
ePTFE grafts (<i>n</i> = 2)	$0.26 \pm 0.09 \times 10^{-2}$	2890 ± 145
Human arteries	8×10^{-2} ⁸	2031–4225 ⁴¹
Human saphenous vein	5×10^{-2} ⁸	1680–2273 ^{42,43}

Our study also indicates that both HBEC and AoSMC preserved their specific cellular phenotype when seeded on the scaffold E. HBEC retained both the expression of Factor VIII-related antigen.⁵³ a classic marker of endothelium, and the binding capacity to Ulex Europaeus I agglutinin, a lectin that selectively recognizes L-fucose moieties of multiple glycoproteins present on the surface of endothelial cells.⁵⁴ AoSMC also maintained their capacity to express smooth muscle α -actin (an early SMC marker) that has been shown to be regulated by hormones, cell proliferation, and altered by pathological conditions including oncogenic transformation and atherosclerosis.⁵⁵

However, analysis of other smooth muscle markers (calponin, caldesmon, calmodulin, tropomyosin, and smoothelin) and long term studies evaluating expression changes at various time points will contribute to clarify whether smooth muscle cells seeded on the nonwoven PET scaffolds retain their full phenotype.

The elastic properties of large arteries and their capacity to synthesize vasoactive substances are key elements for the ability of the arterial wall to function as a modulator of blood pressure and cardiovascular hemodynamics. The scaffold E exhibited compliance and modulus values similar to those reported for human arteries, typically in the order of 8×10^{-2} % mmHg⁻¹, which provides confidence that nonwoven PET fiber grafts can mechanically perform as native vessels. Although other degradable and nondegradable graft prototypes of similar diameters also present vascular-matching compliance values,⁵⁶ this is the first report describing a fabrication method that renders porous scaffolds from PET material (well documented from a clinical and regulatory perspective) with compliance ~7-fold higher than those commercially available obtained from the same material. The burst pressure of scaffold E (~1500 mmHg) was in the order of those reported for the human saphenous vein (1680–2273 mmHg)^{42,43} but slightly below to those of native arteries (~2000–4000 mmHg).⁴¹ However, a body of evidence indicate that the growth of vascular cells within the scaffold under “biomimetic” flow conditions and subsequent collagen deposition^{57,58} can significantly increase their burst strength. This first study on the nonwoven PET scaffolds indicates the potential of these structures for vascular graft applications but further development and optimization of the

protocols to achieve a mature and anatomically/mechanically vascular-matching scaffold are required. This involves the evaluation of various cell seeding, shear-stress, and pulsatile flow protocols and application of various methods that would ensure the penetration of the cells into the structures.

The passive biomechanical properties of the arterial wall are influenced predominantly by the ECM proteins collagen and elastin. Collagen IV is important for the maintenance of integrity and function of basement membranes under conditions of increasing mechanical demands.⁵⁹ Elastin prevents irreversible deformation of the vessel against pulsatile flow.⁶⁰ Alterations in collagen IV and elastin vascular content have been associated to artery stiffening and narrowing during aging and hypertension.^{61,62} HBEC and AoSMC growing on scaffold E expressed collagen and elastin, respectively, indicating that the cells not only preserve their phenotype but they also retain their capacity to produce ECM proteins essential to maintain EC-SMC communication and modulate vascular cellular functions such as cell proliferation, adhesion, and migration.⁶³

The active biomechanical properties of the arterial wall depend on the activation of vascular SMC either directly or through endothelial cell-dependent mechanisms. CGRP is a potent dilator of human brain arteries.⁶⁴ It acts through activation of type II G-protein-coupled receptors located in both EC and SMC and posterior stimulation of adenylate cyclase activity.⁶⁵ Reduction of CGRP release from nerve terminals and down-regulation of CGRP receptor expression in vascular tissues have been reported to be involved in the pathophysiology of hypertension.⁵⁶ EC seeded on scaffold E responded to CGRP producing similar levels of cAMP than those produced by EC seeded on gelatin-coated PFCP. This indicates that the interaction of EC with scaffold E does not alter either the CGRP receptor expression or the dilatory capacity mediated by cAMP formation in the EC.

CONCLUSION

In summary, in this study, using a cost-effective fiber production process, we have produced a novel nonwoven PET fiber scaffold prototype that combines structural, mechanical (compliance matching that of vascular artery) and biocompatibility requirements to be further investigated for small diameter vascular graft applications.

ACKNOWLEDGMENTS

The authors acknowledge the technical support of Mr. Jacques Dufour and Mme Karine Théberge from the National Research Council Canada in the preparation of the nonwoven PET structures.

REFERENCES

1. American Heart Association. Heart Disease and Stroke Statics- 2005 Update. Dallas, Texas.: : American Heart Association; 2005.
2. Niklason LE, Gao J, Abbott WM, Hirschi KK, Houser S, Marini R, Langer R. Functional arteries grown in vitro. Science 1999;284: 489–493.
3. Ghosh J, Baguneid M, Khwaja N, Murphy MO, Turner N, Halka A, Ferguson MW, Kieley CM, Walker MG. Reduction of myointimal

- hyperplasia after arterial anastomosis by local injection of transforming growth factor beta3. *J Vasc Surg* 2006;43:142–149.
4. Devine C, McCollum C. Heparin-bonded Dacron or polytetrafluorethylene for femoropopliteal bypass: Five-year results of a prospective randomized multicenter clinical trial. *J Vasc Surg* 2004;40:924–931.
 5. Tiwari A, Salacinski HJ, Hamilton G, Seifalian AM. Tissue engineering of vascular bypass grafts: Role of endothelial cell extraction. *Eur J Vasc Endovasc Surg* 2001;21:193–201.
 6. Seifalian AM, Tiwari A, Hamilton G, Salacinski HJ. Improving the clinical patency of prosthetic vascular and coronary bypass grafts: The role of seeding and tissue engineering. *Artif Organs* 2002;26:307–320.
 7. Tiwari A, Kidane A, Salacinski H, Punshon G, Hamilton G, Seifalian AM. Improving endothelial cell retention for single stage seeding of prosthetic grafts: Use of polymer sequences of arginine-glycine-aspartate. *Eur J Vasc Endovasc Surg* 2003;25:325–329.
 8. Tai NR, Salacinski HJ, Edwards A, Hamilton G, Seifalian AM. Compliance properties of conduits used in vascular reconstruction. *Br J Surg* 2000;87:1516–1524.
 9. Sarkar S, Salacinski HJ, Hamilton G, Seifalian AM. The mechanical properties of infrainguinal vascular bypass grafts: Their role in influencing patency. *Eur J Vasc Endovasc Surg* 2006;31:627–636.
 10. Williams C, Wick TM. Endothelial cell-smooth muscle cell co-culture in a perfusion bioreactor system. *Ann Biomed Eng* 2005;33:920–928.
 11. Isenberg BC, Williams C, Tranquillo RT. Small-diameter artificial arteries engineered in vitro. *Circ Res* 2006;98:25–35.
 12. Smith MJ, McClure MJ, Sell SA, Barnes CP, Walpoth BH, Simpson DG, Bowlin GL. Suture-reinforced electrospun polydioxanone-elastin small-diameter tubes for use in vascular tissue engineering: A feasibility study. *Acta Biomater* 2008;4:58–66.
 13. Grenier S, Sandig M, Mequanint K. Polyurethane biomaterials for fabricating 3D porous scaffolds and supporting vascular cells. *J Biomed Mater Res A* 2007;82:802–809.
 14. Lee SJ, Oh SH, Liu J, Soker S, Atala A, Yoo JJ. The use of thermal treatments to enhance the mechanical properties of electrospun poly(epsilon-caprolactone) scaffolds. *Biomaterials* 2008;29:1422–1430.
 15. Williamson MR, Black R, Kieley C. PCL-PU composite vascular scaffold production for vascular tissue engineering: Attachment, proliferation and bioactivity of human vascular endothelial cells. *Biomaterials* 2006;27:3608–3616.
 16. Lee SJ, Liu J, Oh SH, Soker S, Atala A, Yoo JJ. Development of a composite vascular scaffolding system that withstands physiological vascular conditions. *Biomaterials* 2008;29:2891–2898.
 17. Vaz CM, van Tuijl S, Bouten CV, Baaijens FP. Design of scaffolds for blood vessel tissue engineering using a multi-layering electrospinning technique. *Acta Biomater* 2005;1:575–582.
 18. Iwasaki K, Kojima K, Kodama S, Paz AC, Chambers M, Umezumi M, Vacanti CA. Bioengineered three-layered robust and elastic artery using hemodynamically-equivalent pulsatile bioreactor. *Circulation* 2008;118(14 Suppl):S52–S57.
 19. Heydarkhan-Hagvall S, Schenke-Layland K, Dhanasopon AP, Rofail F, Smith H, Wu BM, Shemin R, Beygui RE, MacLellan WR. Three-dimensional electrospun ECM-based hybrid scaffolds for cardiovascular tissue engineering. *Biomaterials* 2008;29:2907–2914.
 20. Shinoka T, Shum-Tim D, Ma PX, Tanel RE, Isogai N, Langer R, Vacanti JP, Mayer JE Jr. Creation of viable pulmonary artery autografts through tissue engineering. *J Thorac Cardiovasc Surg* 1998;115:536–545; discussion 545–546.
 21. Shum-Tim D, Stock U, Hrkach J, Shinoka T, Lien J, Moses MA, Stamp A, Taylor G, Moran AM, Landis W, Langer R, Vacanti JP, Mayer JE Jr. Tissue engineering of autologous aorta using a new biodegradable polymer. *Ann Thorac Surg* 1999;68:2298–2304; discussion 2305.
 22. Higgins SP, Solan AK, Niklason LE. Effects of polyglycolic acid on porcine smooth muscle cell growth and differentiation. *J Biomed Mater Res A* 2003;67:295–302.
 23. Rosentman JE, Kempczinski RF, Pearce WH, Silberstein EB. Kinetics of endothelial cell seeding. *J Vasc Surg* 1985;2:778–784.
 24. Hadjizadeh A, Doillon CJ, Vermette P. Bioactive polymer fibers to direct endothelial cell growth in a three-dimensional environment. *Biomacromolecules* 2007;8:864–873.
 25. Palmaz JC, Benson A, Sprague EA. Influence of surface topography on endothelialization of intravascular metallic material. *J Vasc Interv Radiol* 1999;10:439–444.
 26. Dimitrievska S, Petit A, Ajji A, Bureau MN, Yahia L. Biocompatibility of novel polymer-apatite nanocomposite fibers. *J Biomed Mater Res A* 2008;84:44–53.
 27. Ma Z, Kotaki M, Yong T, He W, Ramakrishna S. Surface engineering of electrospun polyethylene terephthalate (PET) nanofibers towards development of a new material for blood vessel engineering. *Biomaterials* 2005;26:2527–2536.
 28. Andrews KD, Feugier P, Black RA, Hunt JA. Vascular prostheses: Performance related to cell-shear responses. *J Surg Res* 2008;149:39–46.
 29. Santhosh Kumar TR, Krishnan LK. Endothelial cell growth factor (ECGF) enmeshed with fibrin matrix enhances proliferation of EC in vitro. *Biomaterials* 2001;22:2769–2776.
 30. Uchida N, Kambic H, Emoto H, Chen JF, Hsu S, Murabayashi S, Harasaki H, Nose Y. Compliance effects on small diameter polyurethane graft patency. *J Biomed Mater Res* 1993;27:1269–1279.
 31. Moreno MJ, Cohen Z, Stanimirovic DB, Hamel E. Functional calcitonin gene-related peptide type 1 and adrenomedullin receptors in human trigeminal ganglia, brain vessels, and cerebromicrovascular or astroglial cells in culture. *J Cereb Blood Flow Metab* 1999;19:1270–1278.
 32. Isenberg BC, Williams C, Tranquillo RT. Endothelialization and flow conditioning of fibrin-based media-equivalents. *Ann Biomed Eng* 2006;34:971–985.
 33. Giudiceandrea ASH, Tai NRM, Punshon G, Hamilton G, Seifalian AM. Development and evaluation of an ideal flow circuit: Assessing the dynamic behavior of endothelial cell seeded grafts. *J Artif Organs* 2000;3:16–21.
 34. Levesque MJ, Nerem RM. The elongation and orientation of cultured endothelial cells in response to shear stress. *J Biomech Eng* 1985;107:341–347.
 35. Wong CS, Sgarioto M, Owida AA, Yang W, Rosenfeldt FL, Morsi YS. Polyethyleneterephthalate provides superior retention of endothelial cells during shear stress compared to polytetrafluoroethylene and pericardium. *Heart Lung Circ* 2006;15:371–377.
 36. Dardik A, Liu A, Ballermann BJ. Chronic in vitro shear stress stimulates endothelial cell retention on prosthetic vascular grafts and reduces subsequent in vivo neointimal thickness. *J Vasc Surg* 1999;29:157–167.
 37. Seifalian AM, Salacinski HJ, Punshon G, Krijgsman B, Hamilton G. A new technique for measuring the cell growth and metabolism of endothelial cells seeded on vascular prostheses. *J Biomed Mater Res* 2001;55:637–644.
 38. Tiwari A, Salacinski HJ, Punshon G, Hamilton G, Seifalian AM. Development of a hybrid cardiovascular graft using a tissue engineering approach. *FASEB J* 2002;16:791–796.
 39. Moreno MJ, Terron JA, Stanimirovic DB, Doods H, Hamel E. Characterization of calcitonin gene-related peptide (CGRP) receptors and their receptor-activity-modifying proteins (RAMPs) in human brain microvascular and astroglial cells in culture. *Neuropharmacology* 2002;42:270–280.
 40. Blondel WC, Lehalle B, Lercher MN, Dumas D, Bensoussan D, Stoltz JF. Rheological properties of healthy and atherosclerotic human arteries. *Biorheology* 2003;40:369–376.
 41. L'Heureux N, Dusserrre N, Konig G, Victor B, Keire P, Wight TN, Chronos NA, Kyles AE, Gregory CR, Hoyt G, Robbins RC, McAllister TN. Human tissue-engineered blood vessels for adult arterial revascularization. *Nat Med* 2006;12:361–365.
 42. L'Heureux N, Paquet S, Labbe R, Germain L, Auger FA. A completely biological tissue-engineered human blood vessel. *FASEB J* 1998;12:47–56.
 43. Lamm P, Juchem G, Milz S, Schuffenhauer M, Reichart B. Autologous endothelialized vein allograft: A solution in the search for small-caliber grafts in coronary artery bypass graft operations. *Circulation* 2001;104(12, Suppl 1):I108–I114.
 44. Jensen N, Lindblad B, Bergqvist D. In vitro attachment of endothelial cells to different graft materials. *Eur Surg Res* 1996;28:49–54.
 45. Kesler KA, Herring MB, Arnold MP, Glover JL, Park HM, Helmus MN, Bendick PJ. Enhanced strength of endothelial attachment on polyester elastomer and polytetrafluoroethylene graft surfaces with fibronectin substrate. *J Vasc Surg* 1986;3:58–64.
 46. White R. The effect of porosity and biomaterial on the healing and long-term mechanical properties of vascular prostheses. *Trans Am Soc Artif Intern Org* 1988;34:95–100.

47. Zhang Z, Wang Z, Liu S, Kodama M. Pore size, tissue ingrowth, and endothelialization of small-diameter microporous polyurethane vascular prostheses. *Biomaterials* 2004;25:177-187.
48. Relou IA, Damen CA, van der Schaft DW, Groenewegen G, Griffioen AW. Effect of culture conditions on endothelial cell growth and responsiveness. *Tissue Cell* 1998;30:525-530.
49. Struijk PC, Stewart PA, Fernando KL, Mathews VJ, Loupas T, Steegers EA, Wladimiroff JW. Wall shear stress and related hemodynamic parameters in the fetal descending aorta derived from color Doppler velocity profiles. *Ultrasound Med Biol* 2005; 31:1441-1450.
50. Abilez O, Benharash P, Mehrotra M, Miyamoto E, Gale A, Picquet J, Xu C, Zarins C. A novel culture system shows that stem cells can be grown in 3D and under physiologic pulsatile conditions for tissue engineering of vascular grafts. *J Surg Res* 2006;132: 170-178.
51. Inoguchi H, Tanaka T, Maehara Y, Matsuda T. The effect of gradually graded shear stress on the morphological integrity of a huvec-seeded compliant small-diameter vascular graft. *Biomaterials* 2007;28:486-495.
52. Gulbins H, Pritisanac A, Petzold R, Goldmund A, Doser M, Dauner M, Meiser B, Reichart B, Daebritz S. A low-flow adaptation phase improves shear-stress resistance of artificially seeded endothelial cells. *Thorac Cardiovasc Surg* 2005;53:96-102.
53. Hormia M, Lehto VP, Virtanen I. Factor VIII-related antigen. A pericellular matrix component of cultured human endothelial cells. *Exp Cell Res* 1983;149:483-497.
54. Holthofer H, Virtanen I, Kariniemi AL, Hormia M, Linder E, Miettinen A. Ulex europaeus I lectin as a marker for vascular endothelium in human tissues. *Lab Invest* 1982;47:60-66.
55. Chaponnier C, Gabbiani G. Pathological situations characterized by altered actin isoform expression. *J Pathol* 2004;204:386-395.
56. Deng PY, Li YJ. Calcitonin gene-related peptide and hypertension. *Peptides* 2005;26:1676-1685.
57. Tschoeke B, Flanagan TC, Koch S, Harwoko MS, Deichmann T, Ella V, Sachweh JS, Kellomaki M, Gries T, Schmitz-Rode T, Jockenhoevel S. Tissue-engineered small-caliber vascular graft based on a novel biodegradable composite fibrin-poly lactide scaffold. *Tissue Eng A* 2009;15: 1909-1918.
58. Hoerstrup SP, Zund G, Sodian R, Schnell AM, Grunenfelder J, Turina MI. Tissue engineering of small caliber vascular grafts. *Eur J Cardiothorac Surg* 2001;20:164-169.
59. Poschl E, Schlotzer-Schrehardt U, Brachvogel B, Saito K, Ninomiya Y, Mayer U. Collagen IV is essential for basement membrane stability but dispensable for initiation of its assembly during early development. *Development* 2004;131:1619-1628.
60. Faury G. Function-structure relationship of elastic arteries in evolution: From microfibrils to elastin and elastic fibres. *Pathol Biol (Paris)* 2001;49:310-325.
61. Arribas SM, Hinek A, Gonzalez MC. Elastic fibres and vascular structure in hypertension. *Pharmacol Ther* 2006;111:771-791.
62. Uspenskaia O, Liebetrau M, Herms J, Danek A, Hamann GF. Aging is associated with increased collagen type IV accumulation in the basal lamina of human cerebral microvessels. *BMC Neurosci* 2004;5:37.
63. Brooke BS, Karnik SK, Li DY. Extracellular matrix in vascular morphogenesis and disease: Structure versus signal. *Trends Cell Biol* 2003;13:51-56.
64. Moreno MJ, Abounader R, Hebert E, Doods H, Hamel E. Efficacy of the non-peptide CGRP receptor antagonist BIBN4096BS in blocking CGRP-induced dilations in human and bovine cerebral arteries: Potential implications in acute migraine treatment. *Neuropharmacology* 2002;42:568-576.
65. Moreno MJ, Stanimirovic DB, Hamel E. CGRP (Calcitonin Gene-Related Peptide). *Encyclopedia of Endocrinology and Endocrine Diseases*, Vol. 1. Academic Press, San Diego; 2004. pp 421-435.